DNS of Thermocapillary Migration of Deformable Droplets

N. Balcázar, O. Antepara, J. Rigola and A. Oliva

1 Introduction

A nonuniform distribution of temperature field on a fluid-fluid interface leads to surface tension gradients, which induce shear stresses that produce the motion of a drop in the direction of the temperature gradient. This phenomenon is known as thermocapillary flow or Marangoni migration. In addition to its importance from a fundamental point of view, thermocapillary flows play an important role in micro gravity environments [1] and micro-devices [2].

Experimental research of these flows has inherent difficulties. However, the development of high-performance computing in combination with Direct Numerical Simulation (DNS) of the Navier–Stokes equations open the possibility to perform controlled numerical experiments, providing a good way to non-invasive measure of droplet flows, although computationally expensive. Multiple methods have been developed for DNS of bubbly (or droplet) flows [3–8], all of them based on the so-called one fluid formulation. In the present work a novel multiple marker level-set method introduced in [9] and extended in [3] to non-isothermal two-phase flows with variable surface tension, is employed for DNS of thermocapillary migration of deformable droplets. Thus, using the conservative level-set approach [4, 6], accumu-

N. Balcázar (✉) · O. Antepara
Termo Fluids S.L., Terrassa, Spain
e-mail: nestor@termofluids.com; nestor@cttc.upc.edu; nestorbalcazar@yahoo.es

O. Antepara
e-mail: oscar@termofluids.com; oscar@cttc.upc.edu

N. Balcázar · O. Antepara · J. Rigola · A. Oliva
Heat and Mass Transfer Technological Center (CTTC),
Technical University of Catalonia (UPC), Barcelona, Spain
e-mail: quim@cttc.upc.edu

A. Oliva
e-mail: cttc@cttc.upc.edu

M. V. Salvetti et al. (eds.), *Direct and Large-Eddy Simulation XI*,
ERCOFTAC Series 25, https://doi.org/10.1007/978-3-030-04915-7_28

lation of mass conservation error inherent to standard level-set methods is avoided. Furthermore, the multiple marker methodology [3, 9] prevents the numerical and potentially unphysical coalescence of the fluid interfaces, taking into account the collision of the droplets, while their volumes are kept constant throughout the simulation [10].

2 Mathematical Model and Numerical Methods

The mathematical formulation has been introduced in our previous work [3], and here is presented for the sake of completeness. The Navier–Stokes equations for the dispersed fluid in Ω_d and continuous fluid in Ω_c are written using the so-called one-fluid formulation, in a global domain $\Omega = \Omega_d \cup \Omega_c$ [3]:

$$\frac{\partial(\rho \mathbf{v})}{\partial t} + \nabla \cdot (\rho \mathbf{v}\mathbf{v}) = -\nabla p + \nabla \cdot \mu \left(\nabla \mathbf{v} + (\nabla \mathbf{v})^T\right) + \rho \mathbf{g} + \mathbf{f}_\sigma(T)\delta_\Gamma, \qquad \nabla \cdot \mathbf{v} = 0 \tag{1}$$

where $\mathbf{v}$ is the fluid velocity, p is the pressure field, ρ is the fluid density, μ is the dynamic viscosity, defined as $\rho = \rho_d H_d + \rho_c(1 - H_d)$ and $\mu = \mu_d H_d + \mu_c(1 - H_d)$, H_d is the Heaviside step function that is one in Ω_d and zero elsewhere, subscripts d and c are used for the dispersed and continuous fluids respectively, $\mathbf{g}$ is the gravitational acceleration, $\mathbf{f}_\sigma$ is the surface tension force, and δ_Γ is the Dirac delta function concentrated at the interface. Furthermore, an energy equation is introduced in order to compute the temperature field (T):

$$\frac{\partial T}{\partial t} + \nabla \cdot (\mathbf{v}T) = \frac{1}{\rho c_p} \nabla \cdot (\lambda \nabla T) \tag{2}$$

where c_p is the heat capacity and λ is the thermal conductivity, defined as $\lambda = \lambda_d H_d + \lambda_c(1 - H_d)$, and $c_p = c_{p,d} H_d + c_{p,c}(1 - H_d)$. A multiple marker level-set method introduced in [4, 9] is used for interface capturing. The ith droplet interface is the 0.5 iso-surface of a level-set function ϕ_i [4], where $i = 1, ..., n_d$ and n_d is the total number of droplets. Since the velocity field is solenoidal, the ith interface transport equation is written in conservative form [3]. Furthermore, a re-initialization equation is solved for steady state, in order to keep a sharp and constant level-set profile [4]:

$$\frac{\partial \phi_i}{\partial t} + \nabla \cdot \phi_i \mathbf{v} = 0, \qquad \frac{\partial \phi_i}{\partial \tau} + \nabla \cdot \phi_i(1 - \phi_i)\mathbf{n}_i = \nabla \cdot \varepsilon \nabla \phi_i \tag{3}$$

Normal vectors $\mathbf{n}_i$ and curvature κ_i at the interface, are computed as $\mathbf{n}_i(\phi_i) = \nabla\phi_i / \|\nabla\phi_i\|$ and $\kappa_i(\phi_i) = -\nabla \cdot \mathbf{n}_i$. The capillary and Marangoni forces [3] are introduced in the context of the continuous surface force model [11], extended to the multiple markers methodology with variable surface tension in [3]:

$$\mathbf{f}_\sigma \delta_\Gamma = \sum_{i=1}^{n_d} (\sigma(T)\kappa_i(\phi_i)\mathbf{n}_i - \nabla\sigma(T) + \mathbf{n}_i(\mathbf{n}_i \cdot \nabla)\sigma(T))\,||\nabla\phi_i|| \tag{4}$$

The fluid properties are regularized by employing a global level-set function for the dispersed phase [9], $H_d = \phi_d$, with $\phi_d = max\{\phi_1, ..., \phi_{n_d-1}, \phi_{n_d}\}$, computing the fluid properties as described in [3]. The mathematical model is discretized using the finite-volume method on a collocated unstructured grid as reported in [3, 4].

3 Numerical Experiments

Validations and verifications of the unstructured multiphase solver used in this work are reported in [4, 9, 10, 12, 13]. Additional validations and verifications are reported in [3] for thermocapillary flows, including the Marangoni migration of $3D$ single and multiple droplets. Thus, this work can be considered as a further step in the understanding of the thermocapillary motion of multiple deformable droplets. Thermocapillary flows ($\mathbf{g} = 0$), are characterized by the thermal conductivity ratio $\eta_\lambda = \lambda_d/\lambda_c$, heat capacity ratio $\eta_{c_p} = c_{p,d}/c_{p,c}$, viscosity ratio $\eta_\mu = \mu_c/\mu_d$, density ratio $\eta_\rho = \rho_c/\rho_d$, Marangoni number $Ma = U_r L_r \rho_c c_{p,c}/\lambda_c$, Capillary number $Ca = U_r\mu_c/\sigma_0$, and Reynolds number $Re = U_r L_r \rho_c/\mu_c$, with $U_r = (\partial\sigma/\partial T)||\nabla T_\infty||(d/2)/\mu_c$, $L_r = d$, dimensionless time $t^* = 2tU_r/d$, dimensionless migration velocity $V_i^* = (\mathbf{e}_y \cdot \mathbf{v}_i)/U_r$, and $\mathbf{v}_i = \int_\Omega \mathbf{v}\phi / \int_\Omega \phi dV$. Material property ratios are 2, unless otherwise stated.

First, a set of two-dimensional experiments is performed. The size of the domain Ω is $(L_x, L_y) = (6d, 12d)$, where d is the initial droplet diameter. No-slip boundary conditions are used at the top and bottom boundaries, whereas Ω is periodic in the $x\text{-}direction$, with $\mathbf{g} = \mathbf{0}$. A linear temperature profile is imposed at the initial time, with a higher temperature at the top boundary, and lower temperature at the bottom boundary. A uniform cartesian mesh with 480×720 cells is employed ($h = d/40$). In the beginning, 18 droplets are distributed randomly in 3 layers of 6 droplets. Figure 1 shows the time evolution of the migration velocity for each droplet, including the effect of Ma, Ca, Re, and bi-dispersion of droplet size. Figures 2 and 3 depict instantaneous snapshots of the droplet distributions, the vorticity, and the Isotherms. Finally, Fig. 4 illustrates the effect of the convective numerical scheme [3, 4] used to discretize the momentum equation and energy equation.

Second, the thermocapillary interaction of 18 droplets is investigated in a $3D$ domain. Ω is a rectangular channel of section $6d \times 6d$ on the plane $x - z$, and length $12d$ on the y-axis. A uniform cartesian mesh of $240 \times 240 \times 480$ cells ($h = d/40$) is employed, distributed in 1536 CPU-cores. No-slip boundary condition is used at the adiabatic lateral walls (x and z directions), a constant temperature is fixed at the top (T_t) and bottom boundaries (T_b), with $T_t > T_b$. At the initial time, 18 droplets are distributed randomly in two layers of 9 droplets, similarly to the arrangement used in [3], for $Re = 40$, $Ma = 60$, $Ca = 0.0416\bar{6}$ with physical property ratios 2.

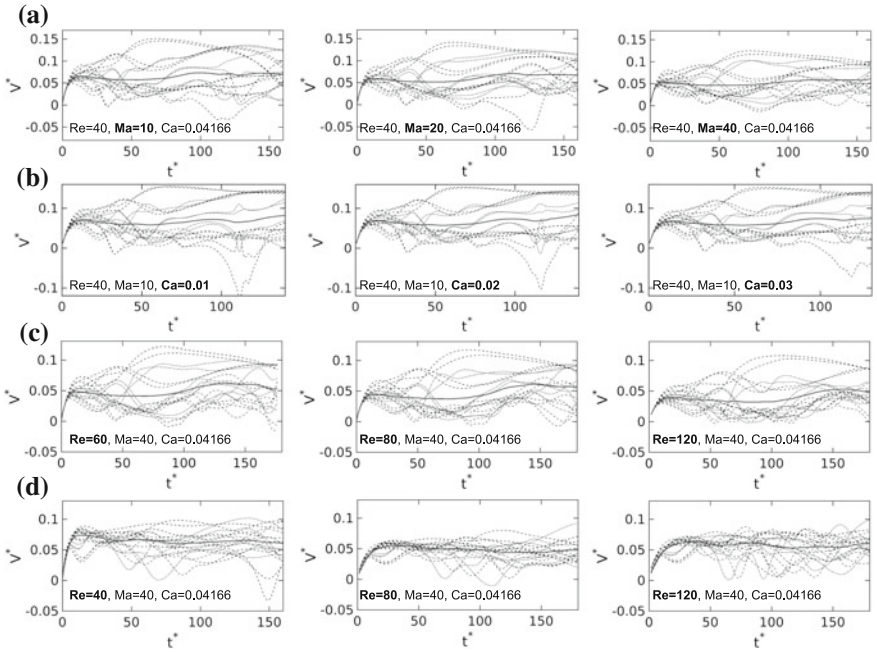

Fig. 1 18 droplets. **a** Effect of Ma. **b** Effect of Ca. **c** Effect of Re. **d** Effect of Re for a bi-dispersed system, with bi-dispersed ratio 0.625. Continuous line for the average velocity. Discontinuous line for each droplet velocity

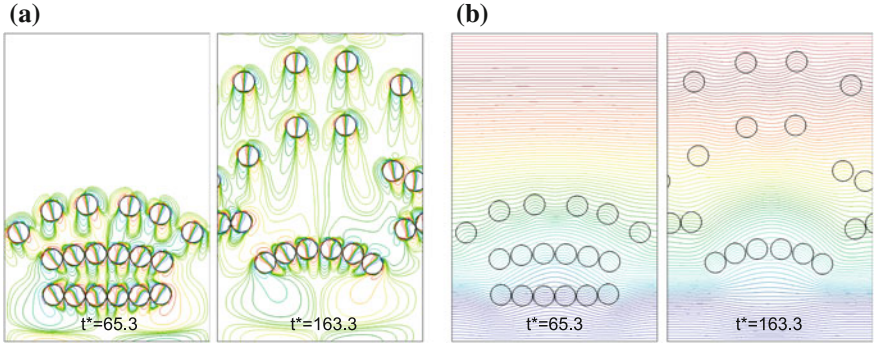

Fig. 2 18 droplets with diameter d, $Re = 40$, $Ma = 10$, $Ca = 0.03$, material property ratios are 2. **a** Vorticity $\mathbf{e}_z \cdot (\nabla \times \mathbf{v})$. **b** Isotherms

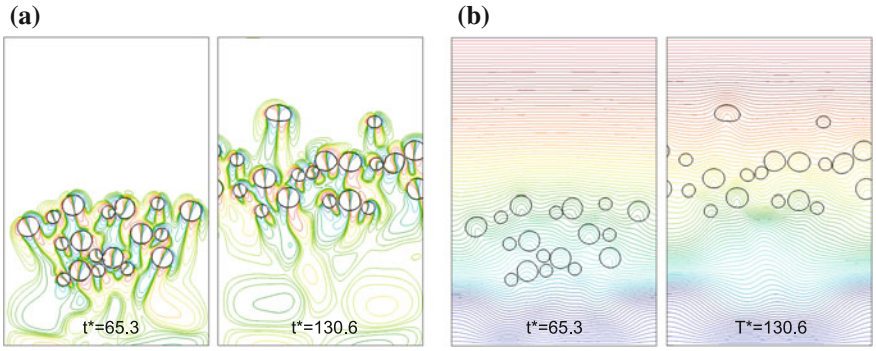

Fig. 3 9 droplets with diameter d, and 9 droplets with diameter $0.625d$, $Re = 40$, $Ma = 10$, $Ca = 0.0416\bar{6}$, material property ratios are 2. **a** Vorticity $\mathbf{e}_z \cdot (\nabla \times \mathbf{v})$. **b** Isotherms

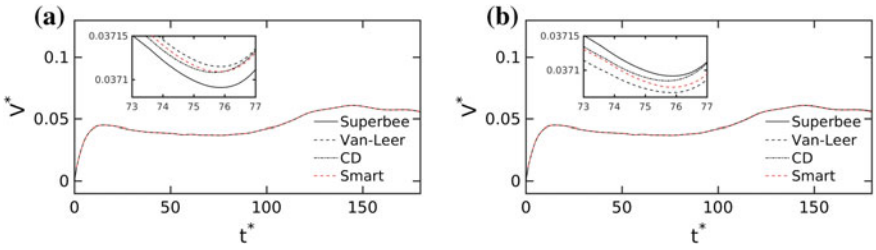

Fig. 4 Effect of convective scheme, flux limiters [3, 4]. Average velocity of 18 droplets, $Re = 80$, $Ma = 40$, $Ca = 0.0416\bar{6}$, material property ratios are 2. **a** Energy equation. **b** Momentum equation

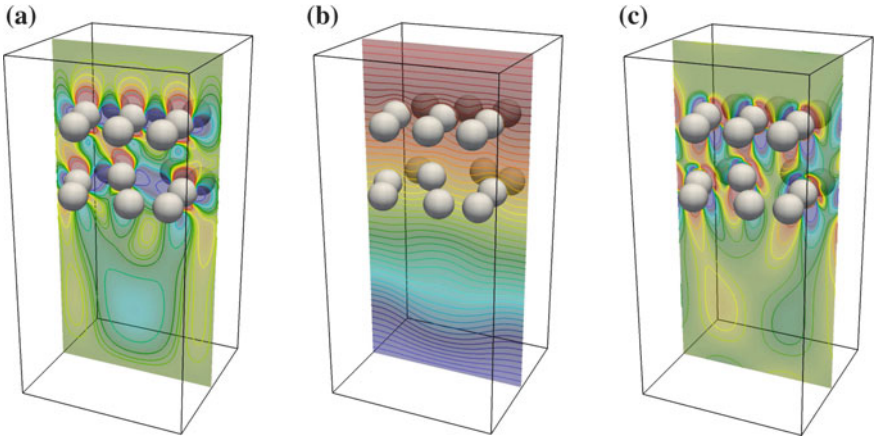

Fig. 5 18 droplets with diameter d, $Re = 40$, $Ma = 60$, $Ca = 0.0416\bar{6}$, material property ratios are 2, $t^* = 111$. **a** Velocity $\mathbf{e}_y \cdot \mathbf{v}$. **b** Isotherms. **c** Vorticity $\mathbf{e}_z \cdot (\nabla \times \mathbf{v})$

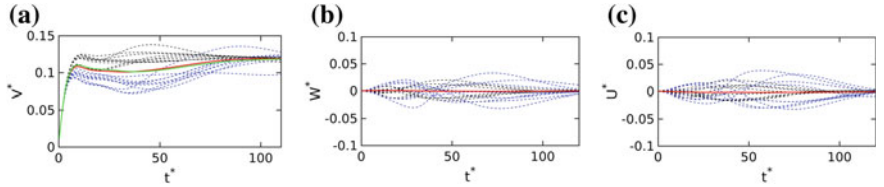

Fig. 6 18 droplets with diameter d, $Re = 40$, $Ma = 60$, $Ca = 0.0416\bar{6}$, material property ratios are 2. First layer of 9 droplets (blue lines), second layer of 9 droplets (black lines), average (red line). Average migration velocity of a second initial condition (green line). $U^* = \mathbf{e}_x \cdot \mathbf{v}_i / U_r$, $V^* = \mathbf{e}_y \cdot \mathbf{v}_i / U_r$, $W^* = \mathbf{e}_z \cdot \mathbf{v}_i / U_r$, $\mathbf{v}_i$ is the droplet velocity

Figure 5 shows the migration velocity $\mathbf{e}_y \cdot \mathbf{v}$, temperature and vorticity $\mathbf{e}_z \cdot (\nabla \times \mathbf{v})$ on the plane $x - y$ of the channel. Furthermore, the time evolution of the ith droplet migration velocity (V^*) is depicted in Fig. 6. This figure also indicates slight sensitivity of the average migration velocity for a different initial droplet distribution. A separation of the two droplet layers is observed, consistently with our previous results [3]. Figure 6 also shows that lateral velocities (U^*, W^*) of the droplets present oscillations, although the average velocity tends to zero.

4 Conclusions

DNS of thermocapillary-driven motion of droplet clouds has been performed using a multiple marker level-set method introduced in our previous works [3, 9], including the effect of Ma, Re and Ca and bi-dispersion of the droplet size, in both $2D$ and $3D$ domains. A repulsion effect arises from the interaction of two-droplets in vertical alignment which induces the formation of horizontal layers. These interactions lead to the random motion of the droplets, however the average velocity of the droplet cloud tend to a quasi-steady state.

Acknowledgements This work has been financially supported by MINECO (ENE2015-70672-P), and by Termo Fluids S.L., Spain. Néstor Balcázar acknowledges financial support of the *Programa Torres Quevedo* MINECO (PTQ-14-07186), Spain. Oscar Antepara acknowledges financial support of MINECO (DI-14-06886), and *Secretaria d' Universitats i Recerca del Departament d'Economia i Coneixement de la Generalitat de Catalunya* (2015DI-68), Spain. Three-dimensional simulations were carried out using computer time awarded by PRACE 14th Call (project 2014112666) on the supercomputer MareNostrum IV based in Barcelona, Spain.

References

1. Subramanian, R.S., Balasubramaniam, R.: The Motion of Bubbles and Drops in Reduced Gravity. Cambridge University Press, Cambridge (2001)
2. Darhuber, A.A., Troian, S.M.: Principles of microfluidic actuation by modulation of surface stresses. Annu. Rev. Fluid Mech. **37**, 425–455 (2005)
3. Balcázar, N., Rigola, J., Castro, J., Oliva, A.: A level-set model for thermocapillary motion of deformable fluid particles. Int. J. Heat Fluid Flow **62, Part B**, 324–343 (2016)
4. Balcázar, N., Jofre, L., Lehmkhul, O., Castro, J., Rigola, J.: A finite-volume/level-set method for simulating two-phase flows on unstructured grids. Int. J. Multiph. Flow **64**, 55–72 (2014)
5. Coyajee, E., Boersma, J.B.: Numerical simulation of drop impact on a liquid-liquid interface with a multiple marker front-capturing method. J. Comp. Phys. **228**, 4444–4467 (2009)
6. Olsson, E., Kreiss, G.: A conservative level set method for two phase flow. J. Comput. Phys. **210**, 225–246 (2005)
7. Sussman, M., Smereka, P., Osher, S.: A level set approach for computing solutions to incompressible two-phase flow. J. Comput. Phys. **144**, 146–159 (1994)
8. Tryggvason, G., Bunner, B., Esmaeeli, A., Juric, D., Al-Rawahi, N., Tauber, W., Han, J., Nas, S., Jan, Y.-J.: A front-tracking method for the computations of multiphase flow. J. Comput. Phys. **169**, 708–759 (2001)
9. Balcázar, N., Lehmkhul, O., Rigola, J., Oliva, A.: A multiple marker level-set method for simulation of deformable fluid particles. Int. J. Multiph. Flow **74**, 125–142 (2015)
10. Balcázar, N., Castro, J., Rigola, J., Oliva, A.: DNS of the wall effect on the motion of bubble swarms. Procedia Comput. Sci. **108**, 2008–2017 (2017)
11. Brackbill, J.U., Kothe, D.B., Zemach, C.: A continuum method for modeling surface tension. J. Comput. Phys. **100**, 335–354 (1992)
12. Balcázar, N., Lehmkhul, O., Jofre, L., Rigola, J., Oliva, A.: A coupled volume-of-fluid/level-set method for simulation of two-phase flows on unstructured meshes. Comput. Fluids **124**, 12–29 (2016)
13. Balcázar, N., Lemhkuhl, O., Jofre, L., Oliva, A.: Level-set simulations of buoyancy-driven motion of single and multiple bubbles. Int. J. Heat Fluid Flow **56**, 91–107 (2015)